ELSEVIER

Contents lists available at ScienceDirect

Acta Biomaterialia

journal homepage: www.elsevier.com/locate/actbio



Full length article

In vitro and in vivo studies of Zn-Mn biodegradable metals designed for orthopedic applications



Bo Jia^{a,1}, Hongtao Yang^{b,c,1}, Yu Han^{a,1}, Zechuan Zhang^b, Xinhua Qu^d, Yifu Zhuang^a, Qiang Wu^a, Yufeng Zheng^{b,**}, Kerong Dai^{a,*}

- ^a Department of Orthopaedic Surgery, Shanghai Key Laboratory of Orthopaedic Implants, Shanghai Ninth People's Hospital, Shanghai Jiaotong University, School of Medicine, Shanghai 200011, PR China
- ^b Department of Materials Science and Engineering, College of Engineering, Peking University, Beijing 100871, PR China
- ^c Department of Plastic & Reconstructive Surgery, The Ohio State University, Columbus, OH 43210, United States
- d Department of Bone and Joint Surgery, Renji Hospital, School of Medicine, Shanghai Jiao Tong University, Shanghai 200127, PR China

ARTICLE INFO

Article history: Received 6 December 2019 Revised 1 March 2020 Accepted 4 March 2020 Available online 9 March 2020

Keywords: Biodegradable metal Zn-Mn alloy Orthopedic implant Osteogenesis

ABSTRACT

In recent years, Zn-based materials provide a new option as biodegradable metals for orthopedic applications. To improve the low strength and brittle nature of pure Zn, small amounts of alloying element Mn (0.1, 0.4 and 0.8 wt.%) were added into Zn to fabricate binary Zn-Mn alloys. An extremely high elongation (83.96 \pm 2.36%) was achieved in the resulting Zn-0.8 wt.%Mn alloy. Moreover, Zn-Mn alloys displayed significantly improved cytocompatibility as compared to pure Zn, according to cell proliferation and morphology analyses. More importantly, a significantly improved osteogenic activity was verified after adding Mn regarding ALP activity and osteogenic expression. Furthermore, Zn-0.8 wt.%Mn alloy scaffolds were implanted into the rat femoral condyle for repairing bone defects with pure Ti as control. Enhanced osteogenic activities were confirmed for Zn-0.8Mn alloy in contrast to pure Ti based on Micro-CT and histological results, and favorable *in vivo* biosafety of Zn-0.8Mn alloy was verified by H&E staining and blood tests. The exceptional mechanical performance and favorable osteogenic capability render Zn-Mn alloy a promising candidate material in the treatment of bone defects or fracture repair.

Statement of Significance

The element Mn, on the one hand, as an essential trace element in the human body, promotes cell proliferation, adhesion, spreading, and regulates bone metabolism; on the other hand, it could significantly improve the ductility of Zn alloys. Here, we systematically reported the biocompatibility and biofunctionality of binary biodegradable Zn-Mn alloys in the bone environment. The Zn-Mn alloys promoted MC3T3-E1 cell proliferation, adhesion, spreading, and osteogenic differentiation *in vitro*. Furthermore, a rat femoral condyle defect model was established; porous Zn-Mn alloy scaffolds were manufactured to repair the bone defects. Significant bone regenerations, considerable bone ingrowth, and desirable biosafety were confirmed *in vivo*. Therefore, biodegradable Zn-Mn with promising osteogenic properties may become new options for orthopedic implant materials.

© 2020 Acta Materialia Inc. Published by Elsevier Ltd. All rights reserved.

1. Introduction

Recently, the medical application prospects of biodegradable metallic materials have attracted widespread attention from material scientists and doctors [1–4]. For instance, Mg-based biodegradable metals have been applied in the field of orthopedic implants; its feasibility in the field of cardiovascular stents has also been extensively studied [5–11]. The Mg-based biodegradable

^{*} Corresponding author. Department of Orthopaedics, Ninth People's Hospital, Shanghai Jiao Tong University, School of Medicine, 639 Zhizaoju Road, Shanghai, 200011. China.

^{**} Co-Corresponding author. Department of Materials Science and Engineering, College of Engineering, Peking University, Beijing 100871, China.

E-mail addresses: yfzheng@pku.edu.cn (Y. Zheng), krdai@163.com (K. Dai).

¹ These three authors contributed equally to this study.

metals have garnered considerable attention in the research of orthopedic implant materials over the last decade, attributing to its good biocompatibility, elastic modulus that closely matches that of the bone tissue, and promising osteogenic activity [12–16]. After more than two decades of developments, biodegradable Mg-based metallic products, including MAGNEZIX screw [17] and Mg-Ca-Zn screws have been used in orthopedics. However, due to the low mechanical strength and rapid degradation rate [18–20], the application of Mg-based biodegradable metals has been dramatically limited to non- or low-load-bearing parts of bones. Although scientists around the world have attempted to improve the mechanical property and degradability of Mg-based biodegradable metal through the alloying, surface coating, and modification [21–25], to date, an ideal solution has not been achieved.

Zn-based biodegradable metals are emerging as a promising alternative to Mg-based biodegradable metals in recent years [3,10,26–29]. Similar to Mg, Zn is an essential trace element in the human body and is involved in basic life processes, such as protein synthesis and energy metabolism [30,31]. It is an essential element in the development of the human immune system and nervous system, and also plays a vital role in bone formation and mineralization processes [32,33]. Bone tissue storage represents 90% of Zn in the human body. Studies have shown that during bone formation, Zn plays a biphasic role in both inhibiting bone resorption by osteoclasts and promoting bone formation by osteoblasts. It also promotes various processes involving osteoblasts, including their proliferation, differentiation, and collagen synthesis [34–37]. These factors suggest the possibility of using Zn-based biodegradable metals as bone implants.

The reported studies on Zn-based biodegradable metals as bone implants are limited to Zn-Mg [38,39], Zn-Ca, Zn-Sr alloy systems [40]. A recent study has shown that the addition of Mn to Zn improved its elongation significantly (elongation>70%) [41], indicating high deformation capability when processing implants with complicated structure design. However, this study on Zn-Mn alloy focused only on material properties, whereas the interactions between Zn-Mn alloy and bone cells and its performance in the bone environment remain unknown. In terms of bone metabolism, Mn regulates bone formation at different scales and levels. Studies have shown that Mn can promote the proliferation, adhesion, and spreading of osteoblasts [42,43], upregulate the expression of marker genes related to bone regeneration, such as alkaline phosphatase (ALP) and bone morphogenetic protein (BMP) [44], promote collagen fiber regeneration and deposition [45], and regulate bone remodeling [46]. It also plays a vital role in the maintenance of bone mass [47]. In an ovariectomized rat model, the supplement of Mn can effectively inhibit bone loss. Besides, Mn salt also exhibits insulin-like effects, which can promote angiogenesis, thereby accelerating the healing of femoral fractures in rats [48,49]. Therefore, based on the favorable biocompatibility and biofunctionality of Mn, the addition of Mn is expected to optimize material properties and improve the biocompatibility of pure Zn.

In this study, various material properties, biocompatibility, and osteogenic functions of Zn-Mn alloys were systematically and comprehensively evaluated *in vitro*. Furthermore, in considering the favorable synergistic osteogenic characteristic of zinc and manganese elements, a rat femoral condyle defect model was established to verify the biosafety and osteogenic activity of a Zn-Mn alloy *in vivo*, to explore the feasibility of its application as an orthopedic implant material.

2. Materials and methods

The experimental design and process are shown in Fig. S1.

2.1. Material and extract preparation

2.1.1. Preparation of Zn-Mn alloys

The metal raw materials used in this study are high-purity Zn (99.99%) and manganese (99.99%) metal blocks, and the binary Zn-Mn alloys were prepared by mixing them at different mass percentages based on needs. The nominal mass fractions of the Mn element used to prepare, Zn-0.1Mn, Zn-0.4Mn, and Zn-0.8Mn alloys were 0.1%, 0.4%, and 0.8%, respectively. The resulting ingots were first thoroughly heat-treated at 350 °C for 48 h and quenched in water before extrusion. Before extrusion, the samples were kept at 260 °C for 2 h. The extrusion was performed at an extrusion ratio of 36 and an extrusion speed of 1 mm/s, to obtain an extruded rod of 10 mm in diameter. The rod sample was then cut into discs (Φ 10 \times 1 mm) and cylinders (Φ 3 \times 4 mm), which were then mechanically polished to 2000 grid. Thereafter, samples were ultrasonically cleaned in acetone and ethanol, and dried at room temperature. Before conducting the cellular and animal experiments, the samples were sterilized with ethylene oxide, which was provided by the Disinfection Supply Center of the Ninth People's Hospital affiliated to the School of Medicine of Shanghai Jiao Tong University, China.

2.1.2. Microstructure characterization and mechanical properties test of Zn-Mn alloys

The disk samples (Φ 10 \times 1 mm) were polished to a mirror surface using a 0.1- μ m diamond polishing paste, then rinsed with deionized water and blown dry. Samples were etched in 4% nitric acid alcohol for 5–10 s, then rinsed with absolute ethanol and blown dry. A scanning electron microscope (SEM, Hitachi S-4800, Japan) equipped with energy dispersive spectrometry (EDS) was used to observe the microstructure of the material and analyze its composition. An X-ray diffractometry (XRD, Rigaku DMAX 2400, Japan) with CuK α target was used to study and determine the microstructure of the material (40 kV, 100 mA, sweep scope of 20–90°, a scan speed of 2°/min, 0.02° step).

The tension and compression testing samples were prepared according to the ASTM-E8-04a and ASTM-E9-89 standards, respectively. A universal material testing machine (Instron 5969, USA) was used to measure the mechanical properties of materials at room temperature. The loading speeds were $1\times 10^{-4}/\mathrm{s}$ and $2\times 10^{-4}/\mathrm{s}$ for tensile and compressive tests, respectively. For each kind of experimental material, the tests and measurements were repeated on five replicate samples for the subsequent statistical analysis. The yield strength was defined as the stress at which 0.2% of plastic deformation occurs on the sample gage length. Ultimate compressive strength was defined as the maximum stress before 50% compressive strain. The microhardness test was adopted by a microhardness tester (SHIMADZUHMV-2t) measuring Vickers hardness with a loading force of 0.1 kN and dwell time of 15 s. An average of at least five measurements was taken for each group.

2.1.3. Electrochemical test

The electrochemical tests were conducted with an electrochemical working station (Autolab, Metrohm, Switzerland) at 37 °C in SBF solution (NaCl 8.035 g/L, NaHCO₃ 0.355 g/L, KCl 0.25 g/L, K₂HPO₄•3H₂O 0.231 g/L, MgCl₂•6H₂O 0.311 g/L, HCl (36–38%) 39 mL/L, CaCl₂ 0.292 g/L, Na₂SO₄ 0.072 g/L, Tris 6.118 g/L, pH 7.4). A three-electrode cell with a counter electrode made of platinum and a saturated calomel electrode (SCE), as the reference electrode, was used. The open-circuit potential (OCP) was monitored for 5400 s for each sample. Electrochemical impedance spectroscopy (EIS) was examined by applying 10 mV perturbation with frequency ranging from 10⁵ Hz down to 10⁻² Hz. Potentiodynamic polarization was carried out at a scan rate of 1 mV/s ranging from –500 mV to 500 mV (vs. OCP), and with a test area of 0.2826 cm².

Table 1The ion concentrations in Pure Zn and Zn-Mn alloys extracts.

Materials	Condition	Zn (µg/mL)	Mn (ng/mL)
Pure Zn Zn-0.1Mn alloy Zn-0.4Mn alloy Zn-0.8Mn alloy	37 ℃ 5% CO ₂	$\begin{array}{c} 12.97\pm0.12 \\ 12.93\pm0.41 \\ 13.62\pm0.36 \\ 12.98\pm0.29 \end{array}$	

Values are expressed as the mean \pm standard error of the mean (n = 5).

Corrosion potential ($E_{\rm corr}$) and corrosion current density ($i_{\rm corr}$) were calculated by linear fit and Tafel extrapolation. An average of at least five measurements was taken for each group.

2.1.4. Immersion corrosion test

Samples were immersed in SBF solutions at 37 °C for 30 days with a solution-to-area ratio of 20 mL/cm² according to ASTM-G31-72. The solution was refreshed every 48 h. After immersion, samples were rinsed with distilled water and air-dried. A solution containing 200 g/L CrO³ was used for cleaning the corrosion products. The corrosion morphologies were observed by SEM both before and after removing the corrosion products. The corrosion rates of samples were calculated according to the equation: $C = \Delta m/\rho At$, where C is the corrosion rate in mm/year, Δm is the weight loss, ρ is the density of the material, A is the initial implant surface area, and t is the implantation time. An average of at least five measurements was taken for each group.

2.1.5. Preparation of Zn-Mn alloy extracts

The extracts were prepared according to the ISO 10,993 standard. Metal discs from each material group were immersed in the α -MEM cell culture medium according to a specific surface area of 1.25 mL/cm². The immersed samples were then placed in a 37 °C environment containing 5% CO₂. After 24 h, the alloy extracts were collected, filtered, and then stored at 4 °C for use within 3 days. The ion concentrations of pure Zn and Zn-Mn alloys extracts are shown in Table 1.

2.2. In vitro cell experiments

In this part of the experiment, the mouse osteogenic precursor cell line MC3T3-E1 was used to evaluate the cytocompatibility and osteogenic activity of pure Zn and Zn-Mn alloys.

2.2.1. Cell culture

Post-resuscitation of MC3T3-E1 cells, the cell suspension was centrifuged, and the supernatant was discarded. The remaining cell pellet was resuspended in the $\alpha\text{-MEM}$ (supplemented with 10% FBS, 1% penicillin (100 U/mL), and streptomycin sulfate (100 mg/mL) (Gibco, Grand Island, NY)) culture medium and placed in a cell culture incubator (37 °C, 5% CO2, and saturated humidity). An optical microscope was used to observe the cells. When cells reach 90% confluency, they were digested with 0.25% trypsin and centrifuged at 300 g for 5 min. The cell pellet was collected and resuspended to a concentration of 3 \times 1010⁴ cells/mL for later use.

2.2.2. Cell proliferation activity and morphology assays

The Cell Counting Kit-8 (CCK-8, Dojindo Molecular Technology, Japan) was used to assess the proliferation activity of MC3T3-E1 cells. The cells were resuspended and counted, and the cell concentration was adjusted to 2×1010^4 cells/mL. Thereafter, equal amounts of cells were seeded in a 96-well plate (100 μ L per well), which was then incubated in a cell culture incubator (37 °C, 5% CO₂, and saturated humidity) for 2–4 h. After the cells attached

to the well bottom, the culture medium was replaced by the alloy extracts (supplemented with 10% FBS, 1% penicillin (100 U/mL), and streptomycin sulfate (100 mg/mL) (Gibco, Grand Island, NY)) of pure Zn, Zn-0.1Mn alloy, Zn-0.4Mn alloy, and Zn-0.8Mn alloy. Given the slow degradation rate of degradable metals in the body and the rapid metabolic exchange of degradation products, the 1-fold and 2-fold diluted extracts were used to evaluate the cytocompatibility. The α -MEM culture medium (supplemented with 10% FBS, 1% penicillin (100 U/mL), and streptomycin sulfate (100 mg/mL) (Gibco, Grand Island, NY)) was used as the blank control. Each group was organized in quintuplicate, which was tested after 1 d, 3 d, 5 d, and 7 d of co-culture. Live/Dead staining and cytoskeletal staining (cytoskeleton labeled with phalloidin, nuclei counterstained with DAPI) were performed on MC3T3-E1 cells co-cultured for 3 days in the 1-fold diluted extract to verify the influence of Zn-Mn alloy extracts on cell viability and morphology, respectively. The stained cells were observed under a confocal laser scanning microscope (CLSM, Leica TCS SP2; Leica Microsystems, Heidelberg, Germany) to assess cell survival and morphology.

2.2.3. Quantitative analysis of ALP activity and staining

The MC3T3-E1 cells were resuspended and counted, and the cell concentration was adjusted to 3×1010^4 cells/mL, which were then seeded in a 6-well plate with 2 mL per well. After 2 h to 4 h of incubation in a cell culture incubator (37 °C, 5% CO2, and saturated humidity), the cells attached to the well bottom and were then observed under a microscope. When cells reach 80% confluency, the culture medium was discarded and replaced with an osteogenic induction solution prepared from the extracts of pure Zn and Zn-Mn alloys. Each group was assayed in triplicates, and the culture solution was refreshed every other day. After 7 d and 14 d of induced differentiation, the osteogenic induction solution was discarded, and cells were rinsed gently with PBS 3 times. The ALP activity of MC3T3-E1 cells was then analyzed quantitatively according to the ALP quantitative analysis kit protocol (Nanjing Jiancheng Bioengineering Institute, China). Also, after 14 days of induced differentiation, the osteogenic induction solution was discarded, and cells were gently rinsed with PBS. The MC3T3-E1 cells from each group were then stained using the ALP staining kit (Shanghai Hongqiao Chemical Reagent Inc., Shanghai, China) and imaged.

2.2.4. Osteogenic-related gene expression detection in MC3T3-E1 cells
Realtime-PCR was used to detect osteogenic-related gene expression in MC3T3-E1 cells. The cells were seeded and cultured, as described above. Based on the ALP activity results, 1-fold and 2-fold diluted Zn-Mn alloy extracts were chosen to prepare the osteogenic induction solution to induce cell differentiation. The cells were observed daily, and the culture solution was refreshed every 2 days.

After 10 days of induced culture, the culture medium was discarded. Total RNA was then extracted using the RNeasy mini kit (Qiagen) according to the manufacturer's instructions. With β actin as the internal reference, the mRNA expression levels of the marker genes (ALP, OCN, RunX-2, and Col I) in MC3T3-E1 cells were measured using the RT-PCR method. Primer sequences are shown in Table 2. A reverse transcription kit (SuperScriptTM III Reverse Transcriptase) was used to reverse 1 mg RNA., The SYBR Premix Ex Taq II $(2\times)$ was used as the PCR reagent to perform RT-PCR in the ABI 7500 Fast machine (Applied Biosystems, Courtaboeuf, France). The reaction conditions were as follows: 95 °C 30 s; 95 °C 5 s + 60 °C 40 s, 40 cycles; dissolution curve, 95 °C 15 s + 60 °C 1 min + 95 °C 15 s. The $2^{-\Delta \Delta Ct}$ method was applied to calculate the results. $\Delta\Delta$ Ct = (average Ct value of target gene in the test group - average Ct value of internal reference gene in the test group) - (average Ct value of target gene in the control

Table 2 Primer sequence of MC3T3-E1 cells.

Target gene	Direction	Primer sequence (5'-3')
ALP	Forward	GGAGATGGTATGGGCGTCTC
	Reverse	GGACCTGAGCGTTGGTGTTA
Col I	Forward	TTCTCCTGGCAAAGACGGAC
	Reverse	CTCAAGGTCACGGTCACGAA
OCN	Forward	CTGACCTCACAGATCCCAAGC
	Reverse	TGGTCTGATAGCTCGTCACAAG
Runx-2	Forward	TCGGAGAGGTACCAGATGGG
	Reverse	AGGTGAAACTCTTGCCTCGT

group — average Ct value of internal reference gene in the control group).

2.3. In vivo repair of rat femoral condyle defect with Zn-Mn alloys

2.3.1. Implants selection and preparation

According to the aforementioned in vitro experimental results, Zn-0.8Mn alloy displayed the ideal performance. Therefore, in this part of the experiment, Zn-0.8Mn alloy was selected for the in vivo osteogenic activity and biosafety assessment. In the selection of the control material, we firstly considered pure Zn. However, in our previous bone environment studies of zinc-based biodegradable metals [38,50,51], delayed osteointegration, poor bone regeneration and obvious inflammatory were found after pure Zn rods implanted into the rats' femoral condyle. Therefore, in order to evaluate the orthopedic application feasibility and bone defect repair activity of Zn-Mn alloys, the golden standard material for clinical orthopedic repair of large bone defects, pure Ti, was selected as the control in this study. The materials were prepared into cylindrical samples (3 mm in diameter and 4 mm in height). Laser cauterization (TruLaser Tube 5000 fiber, Germany) was applied to create equal numbers of through-holes (0.5 mm in diameter) in the samples, thereby shaping the materials into porous bone repair scaffolds (porosity 30.85 \pm 0.296%).

2.3.2. Surgical procedure

All animal operations and experiments were approved by the Animal Ethics Committee of the Ninth People's Hospital affiliated to Shanghai Jiao Tong University. A rat femoral condyle defect repair model was established, and the surgeries were performed under sterile conditions. In this part of the experiment, a total of 30 male rats at 12 weeks old (average weight of 293 g \pm 23.5 g) were used. The rats were anesthetized by intraperitoneal injection with ketamine (10 mg/kg, Shanghai Ziyuan Pharmaceutical Co., Ltd, Shanghai, China) and 2% xylazine (5 mg/kg, Bayer, Leverkusen, North Rhine-Westphalia, Germany). The skin of the rat's right hind limb was prepared, and the knee joint was fixed. After that, a longitudinal incision of approximately 15 mm was made lateral to the patellar ligament. The lateral femoral condyle was then exposed by blunt separation. A 3-mm drill bit was used to introduce a cylindrical bone defect of 3 mm in diameter and 4 mm in depth. The defect site was rinsed with saline and a scaffold was implanted. The surgery site was rinsed with saline again and the incision was closed by suturing layer by layer. Buprenorphine (Temgesic, Reckitt & Cloman, Hull, UK) was injected subcutaneously at a dose of 0.3 mg/kg for postoperative analgesia. The surgical operation groups were as follows: (1) The pure Ti control group used porous pure Ti scaffolds to repair the bone defects in a total of 15 rats. 5 rats were euthanized every 4 weeks (after 4 weeks, 8 weeks, and 12 weeks of implantation) to collect the scaffolds; (2) The Zn-0.8Mn alloy experimental group used porous Zn-0.8Mn alloy scaffold to repair the bone defects in a total of 15 rats. Five rats were euthanized every 4 weeks (after 4 weeks, 8 weeks, and 12 weeks of implantation).

Table 3 Details of the scanning procedure.

Tube voltage (kVp)	Tube current (μA)	Resolution (μm)	Exposure time (ms)
70	200	14.8	300

2.3.3. Micro-CT evaluation of the osteogenic properties of Zn-0.8Mn alloy in vivo

Subgroups of experimental animals from each group were euthanized at 4 weeks, 8 weeks, and 12 weeks post-surgery. The whole right femurs of the rats were retrieved and fixed with 4% paraformaldehyde. Micro-CT (Scanco Micro-CT100, Switzerland) was used to scan the distal femur and femoral condyle. The detailed scanning parameters are shown in Table 3. Thereafter, the Scanco µ100 evaluation software was used to perform 3D reconstruction to evaluate the osteogenic activity and degradation behavior of the Zn-0.8Mn alloy scaffold *in vivo*.

2.3.4. Cross-sectional and histomorphometric analysis

After completing the Micro-CT scan, hard-tissue slicing was performed on the rat femur specimen. The specimen was first fixed, then rinsed in water, dehydrated in ethanol, cleaned in xylene, and finally, embedded in methyl methacrylate. For each specimen, 4-5 slices were made by cutting along the sagittal plane of the femur's long axis, vertical to the implant in the femoral condyle. Then one slice of each specimen was polished to 7000 grit; the crosssections were observed by an SEM (Hitachi S-4800, Japan) with EDS. The rest slices were then ground and polished to a thickness of 100 µm, and three slices were selected to perform Van Gieson, Toluidine blue, and Paragon staining. After the staining process, a high-resolution microscope (Olympus CKX41, Olympus Co., Ltd., Tokyo, Japan) was used to observe and image the slices. Three images were obtained for each slice, namely a full-view image of the bone defect areas at a low (20 \times), medium (50 \times), and high magnification (100 \times). Low magnification (20 \times) images of the Van Gieson staining were chosen to analyze the new bone mass semiquantitatively using the Image-Pro-Plus 6.0 software (Media Cybernetics, Inc., Rockville, MD, USA).

2.3.5. Assessment of general conditions and in vivo biosafety of experimental animals

The general postoperative conditions of the experimental animals, including body temperature, body weight, and wound healing conditions, were observed daily. At 12 weeks postoperatively, rat arterial blood samples were obtained from both the pure Ti control group and the Zn-0.8Mn alloy experimental group randomly using the cardiac blood sampling method. The concentrations of Zn²⁺ and Mn²⁺ in the serum were measured using ICP-mass spectrometry (ICP-MS, NexION 300Â, USA). At the same time, at 12 weeks postoperatively, samples were collected from the heart, liver, spleen, lung, and kidney of rats in both the pure Ti control group and the Zn-0.8Mn experimental group. The concentrations of Zn²⁺ and Mn²⁺ in these organs were also measured using ICP-mass spectrometry (ICP-MS, NexION 300Â, USA). The organ tissues were fixed, embedded, and stained using hematoxylin and eosin (H&E) to observe possible pathological changes in the organs.

2.4. Data analysis

The SPSS 25.0 statistical software (SPSS Inc., Chicago, USA) was used to analyze the data. All quantitative data are presented as Mean \pm SD. The data were analyzed using the independent sample t-test and one-way analysis of variance (ANOVA), with $^*p < 0.05$ or $^{**}p < 0.01$ as the threshold for determining the statistical significance of the difference.

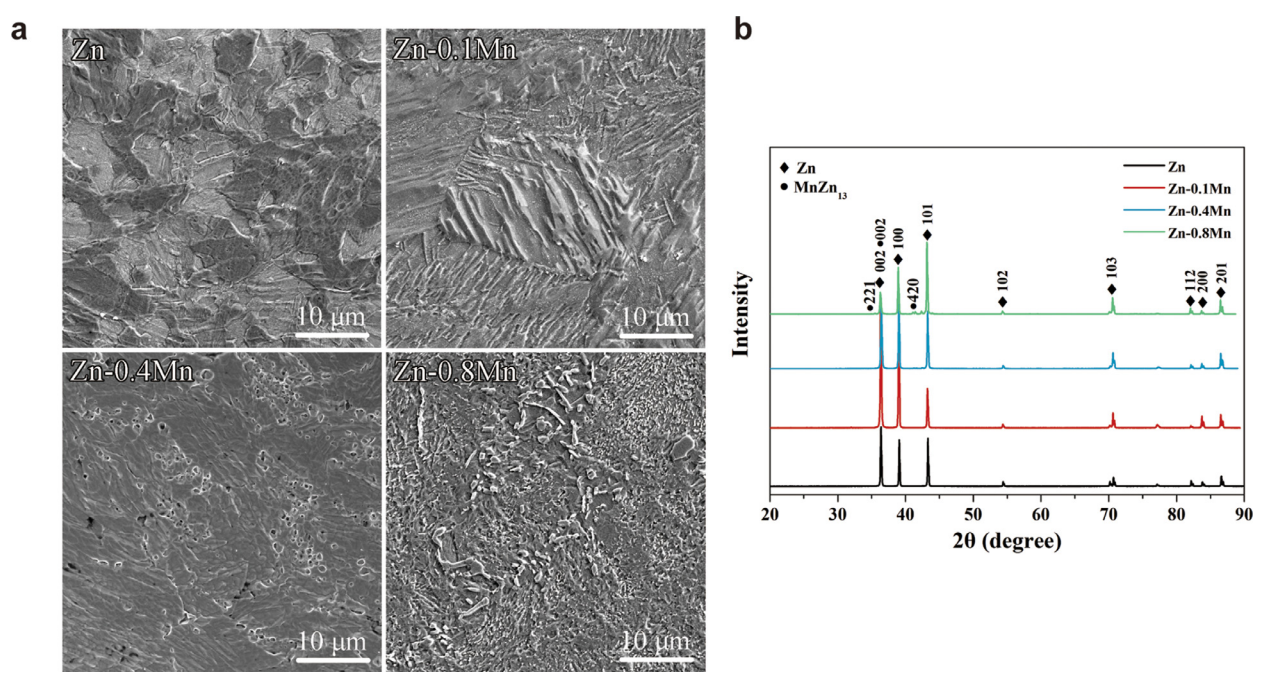


Fig. 1. The microstructure of pure Zn and Zn-Mn alloys. (a) SEM images and (b) X-ray diffraction.

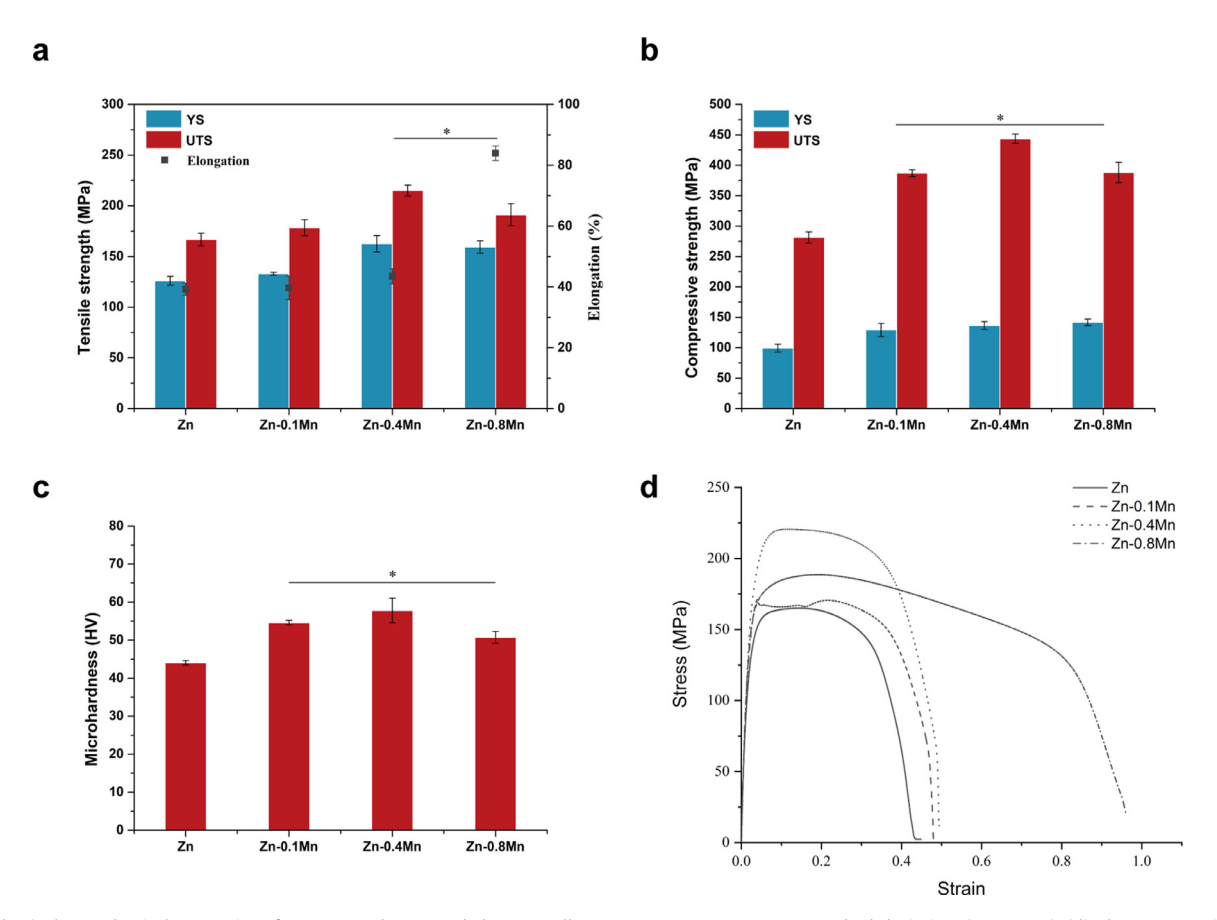


Fig. 2. (a, b, c) The mechanical properties of pure Zn and as-extruded Zn-Mn alloys. Data represent mean \pm standard deviation, (*p < 0.05). (d) The stress-strain behavior of pure Zn and as-extruded Zn-Mn alloys.

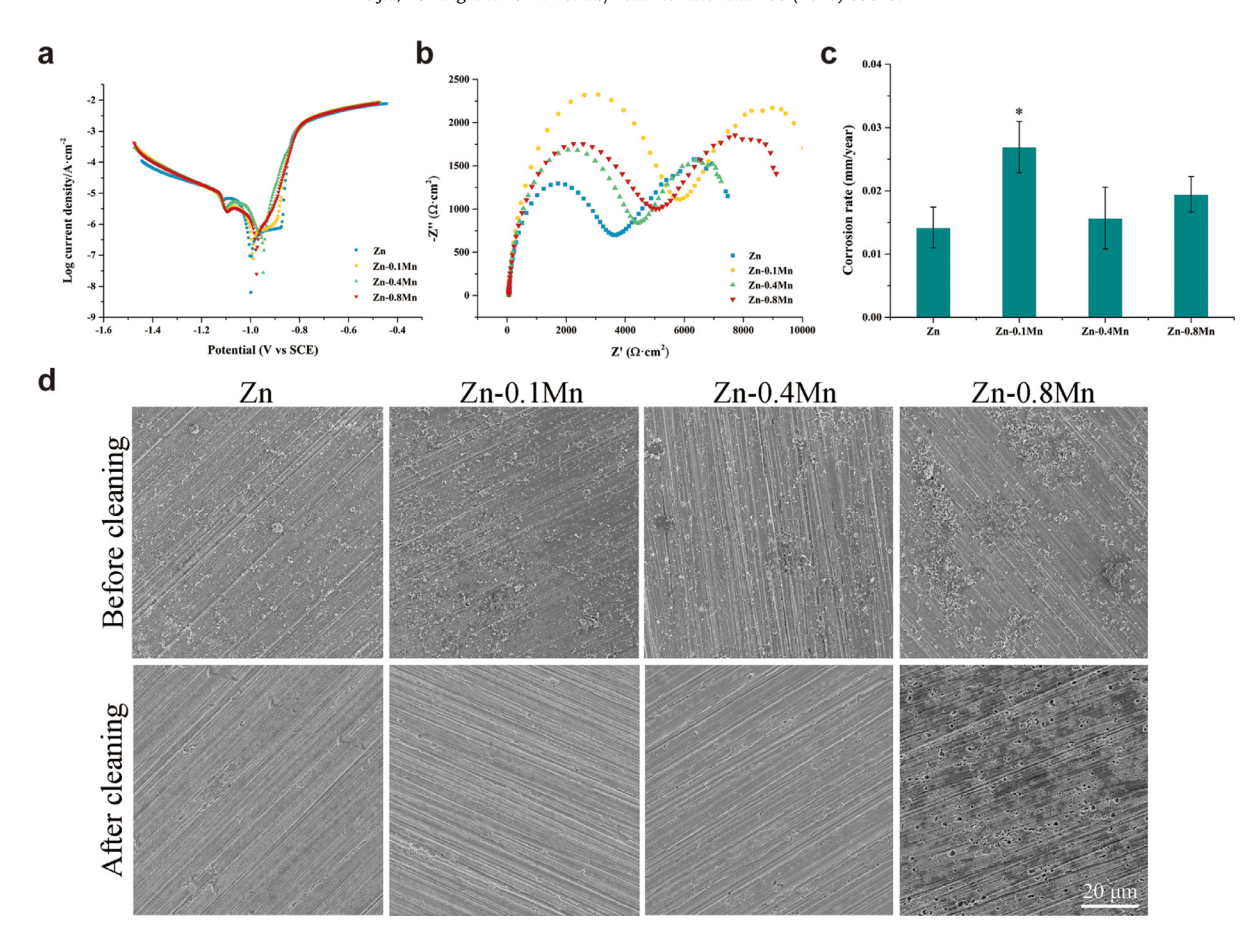


Fig. 3. In vitro corrosion results of Zn-Mn alloys. (a) Polarization curves, (b) EIS and (c) corrosion rates of pure Zn and Zn-Mn alloys. (d) The corrosion morphology of experimental samples after immersion in the SBF solution for 30 days. Data represent mean \pm standard deviation. (*p < 0.05).

Table 4 Electrochemical parameters for Zn-Mn alloys in the SBF solution (37 \pm 0.2 °C).

Materials	$I_{\rm corr}~(\mu \text{A}\cdot\text{cm}^{-2})$	$E_{\rm corr}$ (V)	Corrosion rate (mm·year ⁻¹)
Pure Zn	9.031 (1.011)	-0.999 (0.004)	0.269 (0.031)
Zn-0.1Mn alloy	5.396 (0.259)*	-0.964 (0.049)	0.161 (0.008)*
Zn-0.4Mn alloy	10.671 (3.034)	-0.942 (0.028)	0.318 (0.122)
Zn-0.8Mn alloy	7.436 (0.753)	-0.976 (0.008)	0.111 (0.011)

Numbers in the brackets represent the standard deviation, p < 0.05.

3. Results

3.1. Material characterization

3.1.1. Microstructure and mechanical properties

The metallography of pure Zn and Zn-Mn alloys is presented in Fig. 1. Pure Zn showed an average grain size of around 10 μm . The intermetallic phase was almost invisible in Zn-0.1Mn alloy, while a tiny phase was found after adding 0.8 wt.% of Mn. X-ray diffraction identified the intermetallic phase as MnZn13. The mechanical property and the stress-strain behavior of as-extruded Zn-Mn alloys are shown in Fig. 2. Zn-Mn alloys possessed significantly higher strength and microhardness than that of pure Zn. More importantly, the elongation to failure of Zn-0.8Mn alloy reached 83.96 \pm 2.36%

3.1.2. In vitro corrosion behavior

Polarization curves and EIS (Fig. 3a and b) were performed to evaluate the corrosion behavior of Zn-Mn alloys. The calculated electrochemical parameters are shown in Table 4. Alloying with Mn showed little impact on the corrosion potential and corrosion cur-

rent density of Zn. The corrosion morphology of experimental samples after immersion in an SBF solution for 30 days was shown in Fig. 3. Pure Zn was almost intact after immersion. Zn-0.1Mn and Zn-0.4Mn alloys exhibited corrosion morphology similar to that of pure Zn, whereas many pits were found in Zn-0.8Mn alloy after removal of corrosion products. The corrosion rates calculated from weight loss indicated accelerated corrosion after adding Mn.

3.2. In vitro cytocompatibility evaluation results of Zn-Mn alloys

The MC3T3-E1 cell viability after co-culture for 1 d. 3 d. 5 d. and 7 d in various extracts was examined using the CCK-8 method (Fig. 4). From the experiment using the 1-fold diluted extract, the pure Zn group showed significantly reduced cell viability starting from the first day, compared to the blank control group. However, Zn-Mn alloy groups only showed slight cell viability decreases on the first day. On the following days, at 3 d, 5 d, and 7 d, cell viability all showed significant increases compared to the blank control group. Among them, the Zn-0.4Mn and Zn-0.8Mn alloy groups showed the most significant increases. Similar phenomena were observed in the experiment using the 2-fold diluted extract, such that the pure Zn group exhibited weaker cell viability than the blank control group at 1 d, 3 d, 5 d, and 7 d; the Zn-Mn alloy groups showed similar cell viability as the blank control group on 1 d, except for the Zn-0.8Mn alloy group, which showed slightly lower cell viability than the blank control group at 1 d. However, on the following days at 3 d, 5 d, and 7 d, the cell viability in the Zn-Mn alloy groups all improved compared to the pure Zn group, with the Zn-0.4Mn and Zn-0.8Mn alloy groups exhibiting the most significant increases. Therefore, according to ISO 19,003-5 standards, it can be said that pure Zn is cytotoxic to MC3T3-E1

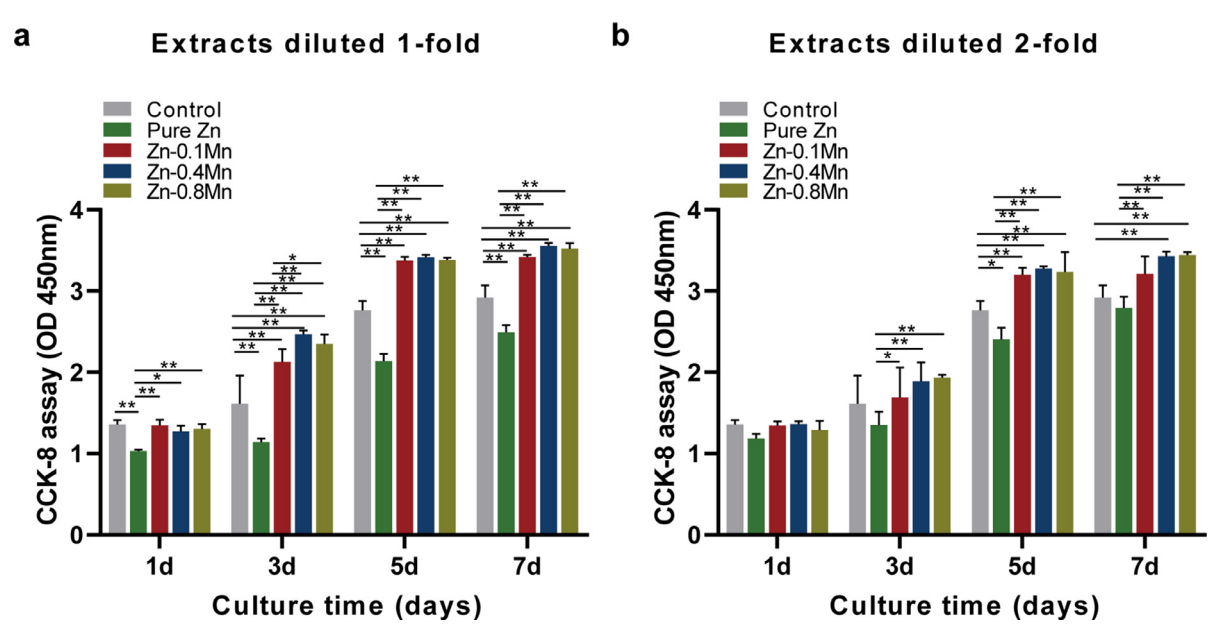


Fig. 4. The MC3T3-E1 cells activity after co-culture for 1d, 3d, 5d, and 7d in pure Zn and Zn-Mn alloy extracts (a) $1 \times$ and (b) $2 \times$ dilutions. Data represent mean \pm standard deviation. (*p < 0.05; ** p < 0.01).

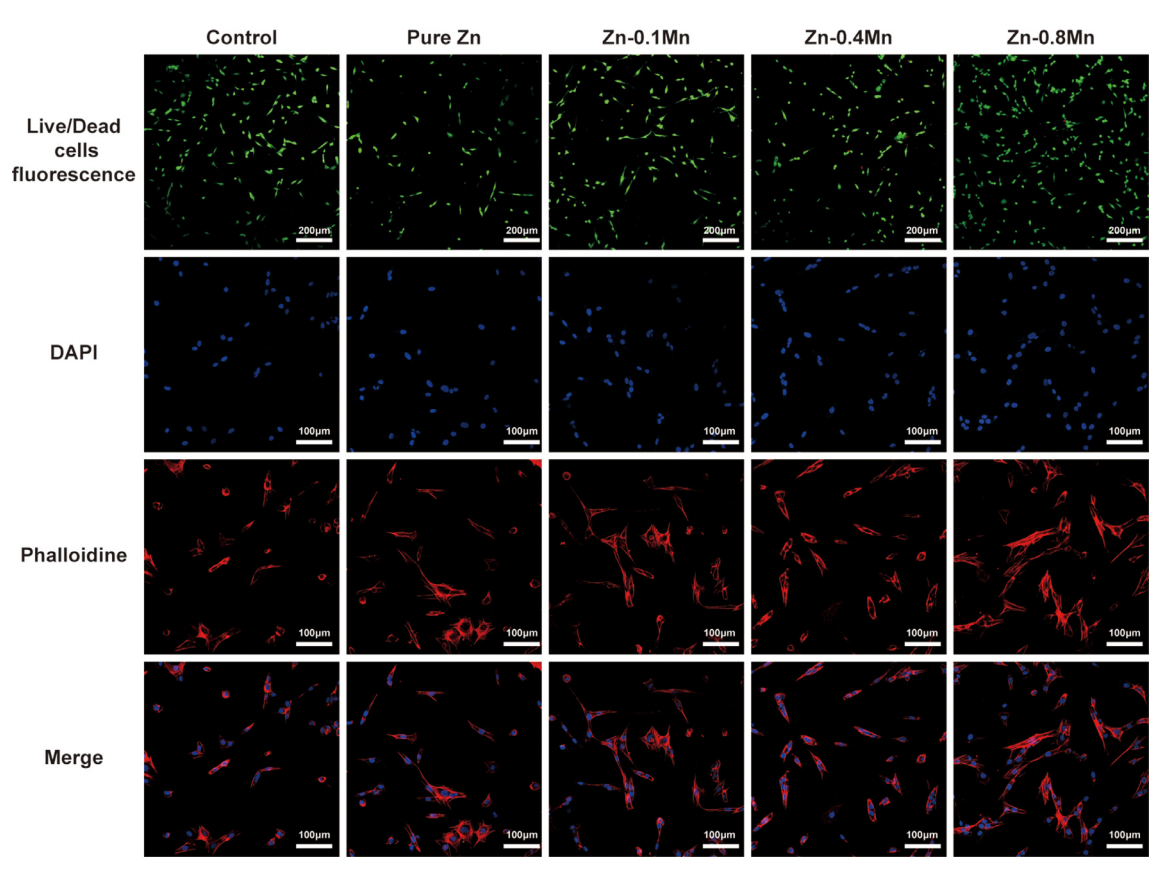


Fig. 5. Live/dead cell staining and cytoskeletal staining for MC3T3-E1 cells cultured with pure Zn and Zn-Mn alloy extracts (1× dilution). Live cells exhibit green fluorescence, while dead cells exhibit red fluorescence in live/dead cell staining. Representative images of cells stained with phalloidine for actin filaments (red) and DAPI for cell nuclei (blue). (For interpretation of the references to colour in this figure legend, the reader is referred to the web version of this article.)

cells, but the addition of alloying element Mn can significantly improve the cytocompatibility of pure Zn.

Next, in order to verify the cell viability in each group more intuitively, the influence of alloy extracts on MC3T3-E1 cell viability was examined by means of Live/Dead and cytoskeletal staining. As shown in Fig. 5, in Live/Dead staining, the number of viable

cells was significantly lower in the pure Zn group compared to the blank control group, while the number of viable cells in the Zn-0.8Mn alloy group increased significantly. No dead cells were observed in any of the groups. The Zn-Mn alloy groups showed significant improvements compared to the pure Zn group. Phalloidin staining indicated a slightly poorer spread in the pure Zn

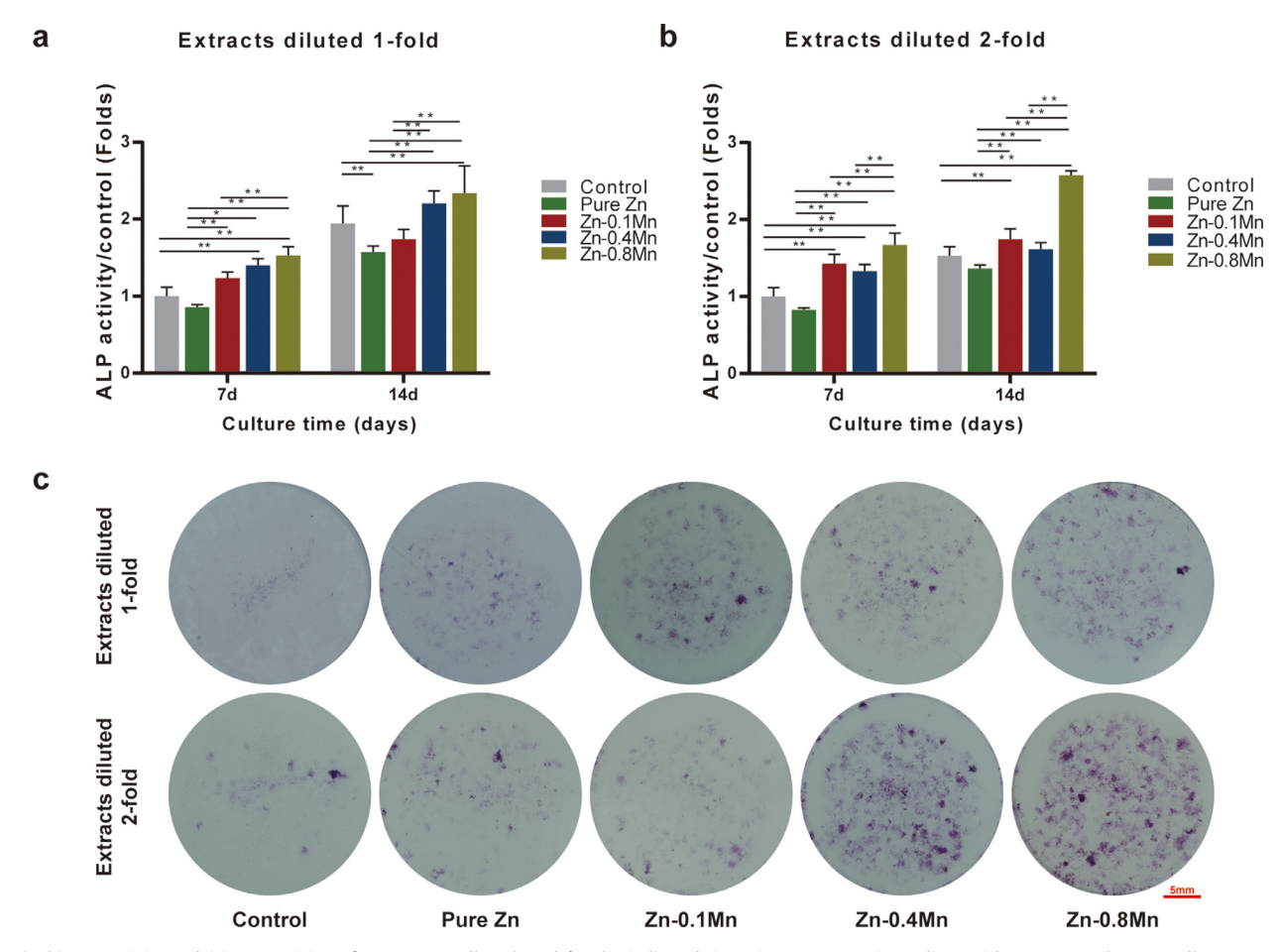


Fig. 6. (a, b) ALP activity and (c) ALP staining of MC3T3-E1 cells cultured for the indicated times in an osteogenic medium with pure Zn and Zn-Mn alloys extracts. Data represent mean \pm standard deviation. (*p < 0.05; ** p < 0.01).

group, while other groups displayed suitable morphologies, with the Zn-0.8Mn alloy group displaying the best morphology. The above results demonstrate the cytotoxicity of pure Zn to MC3T3-E1 cells; however, the addition of alloying element Mn significantly improves the cytocompatibility of pure Zn. Among all alloy groups, the Zn-0.8Mn alloy showed the best cytocompatibility, which is consistent with the CCK-8 results.

3.3. In vitro osteogenic differentiation activity evaluation of Zn-Mn alloys

Quantitative analysis of ALP activity of MC3T3-E1 cell osteogenic differentiation induced by alloy extracts is shown in Fig. 6a and b. The results showed that in the experiment using 1-fold diluted extract, the pure Zn group exhibited the lowest ALP expression at both 7 d and 14 d. At 7 d, ALP expression levels of Zn-Mn alloy groups were higher than that of the blank control group, where the Zn-0.8Mn alloy group had the highest ALP expression. At 14 d, the Zn-0.4Mn and Zn-0.8Mn alloy groups had higher ALP expression levels than the control group, and the Zn-0.8Mn alloy group still expressed the highest ALP expression. In the experiment using 2-fold diluted extracts, the pure Zn group still displayed the lowest ALP expression, while the Zn-0.8Mn alloy group displayed the highest ALP expression. The results showed that pure Zn extract exerted an inhibitory effect on osteogenic differentiation of MC3T3-E1 cells, while the Zn-0.8Mn alloy group exerted a significant promoting effect.

Next, ALP staining was performed on the extract-induced differentiated cells, and the results are shown in Fig. 6c. In the experiment using 1-fold diluted extracts, compared to the control group and the pure Zn group, the Zn-Mn alloy groups showed significantly enhanced ALP staining. In the experiment using 2-fold diluted extracts, the trend was further evident, especially in the Zn-0.4Mn alloy and the Zn-0.8Mn alloy groups, which showed significantly higher expression levels. This showed that Zn-0.4Mn and Zn-0.8Mn alloy extracts retain visible osteogenic capabilities. Fig. 7 shows the expressions of osteogenic differentiation-related genes (ALP, Col I, OCN, and Runx-2) in each group after osteogenic induction. The results are consistent with previous experiments, which showed that Zn-Mn alloy groups significantly improved osteogenic capability compared to the control and pure Zn groups, among which the Zn-0.8Mn alloy group showed the most significant improvement.

3.5. In vivo osteogenic properties and biosafety evaluation of Zn-0.8Mn alloy

3.5.1. Micro-CT results

Fig. 8 shows the three-dimensional, sagittal, and coronal reconstruction micro-CT images (at 4 weeks, 8 weeks, and 12 weeks, respectively) of the rat femoral condyle defects repaired by scaffolds prepared from Zn-0.8Mn alloy and pure Ti (control group). At 4 weeks postoperatively, a small amount of new bone formation (shown by red arrows) could be observed around the pure Ti and Zn-0.8Mn alloy scaffold on the sagittal and coronal images. Also, degradation products can be seen around the Zn-0.8Mn alloy scaffold (shown by yellow arrows). At 8 weeks postoperatively, new bone tissues can be seen around the pure Ti scaffold (shown by red arrows), while numerous new bone tissues can be seen around the Zn-0.8Mn alloy scaffold (shown by red arrows), where the new

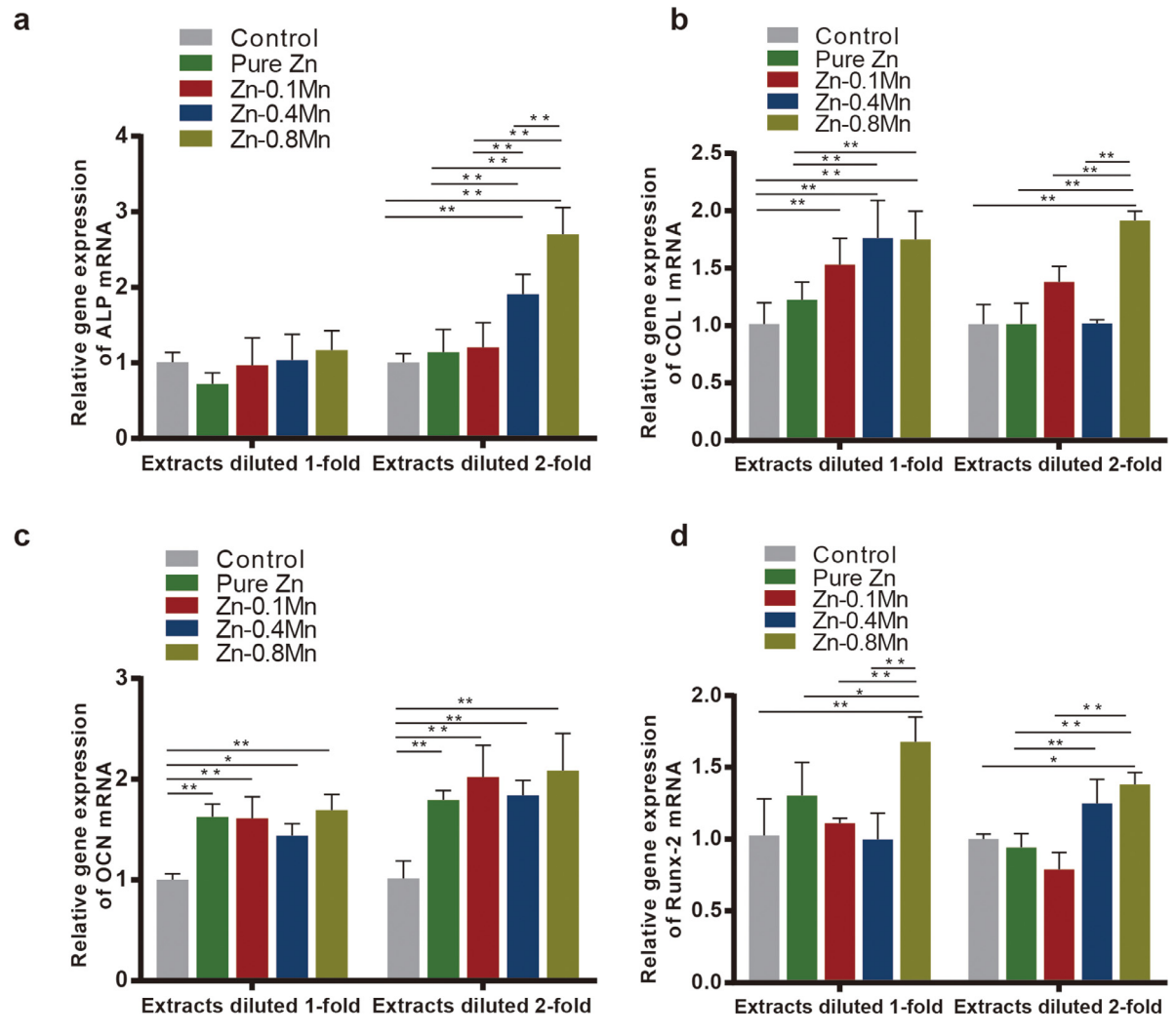


Fig. 7. The relative expression of (a) ALP, (b) COL I, (c) OCN, (d) Runx-2 in MC3T3-E1 cells cultured for 10days in an osteogenic medium with pure Zn and Zn-Mn alloys extracts ($1 \times$ and $2 \times$ dilutions). Data represent mean \pm standard deviation. (*p < 0.05; ** p < 0.01).

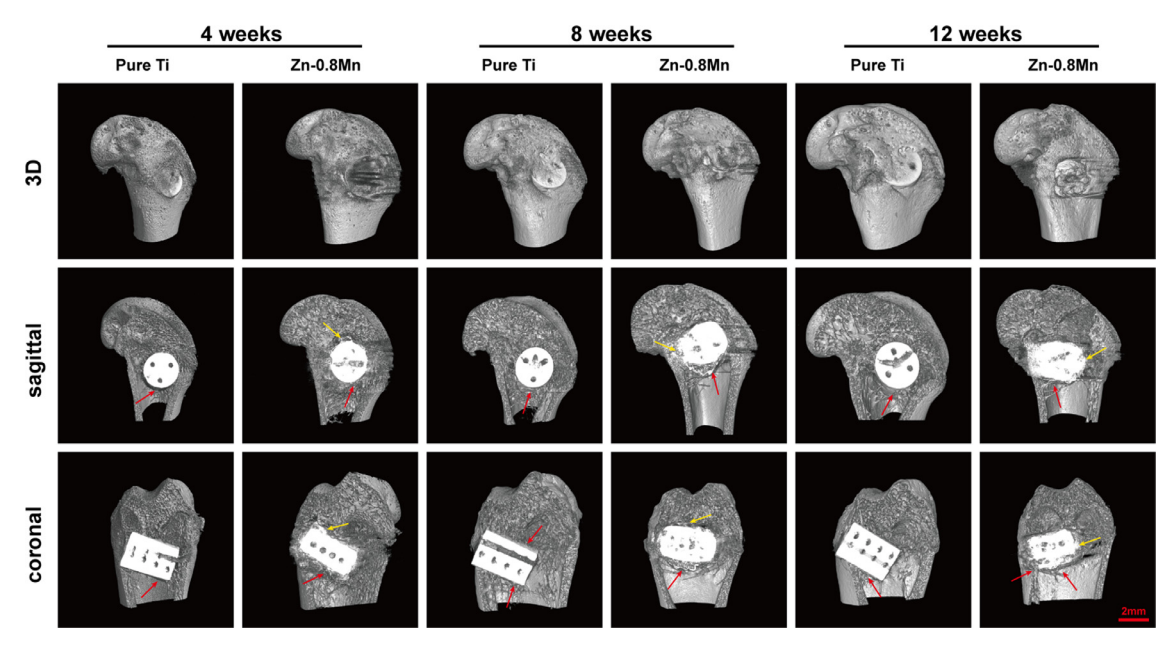


Fig. 8. Three-dimensional, sagittal, and coronal reconstruction micro-CT images of the rat femoral condyle at 4 weeks, 8 weeks, and 12 weeks after surgery. The red arrows indicate new bone while the yellow arrows indicate degradation products of Zn-0.8Mn alloy scaffolds. (For interpretation of the references to colour in this figure legend, the reader is referred to the web version of this article.)

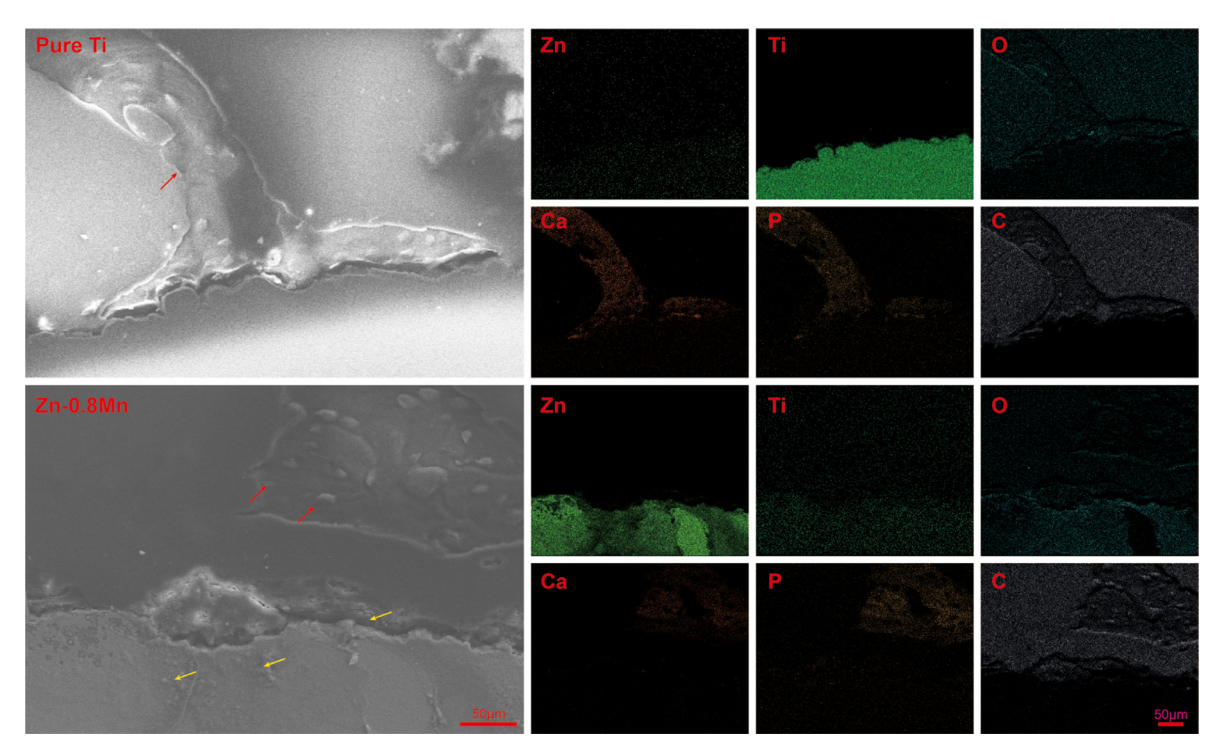


Fig. 9. The EDS mapping of pure Ti and Zn-0.8Mn alloy (12weeks after surgery), maps of elements zinc, titanium, oxygen, calcium, phosphate, and carbon are in green, dark green, light blue, orange, yellow and gray, respectively. The red arrows indicate new bone while the yellow arrows indicate degradation products of Zn-0.8Mn alloy scaffolds. (For interpretation of the references to colour in this figure legend, the reader is referred to the web version of this article.)

trabecular bone was also thicker than that in the pure Ti group. Simultaneously, increased degradation products can be observed around the Zn-0.8Mn alloy scaffold (shown by yellow arrows). At 12 weeks postoperatively, new bone tissues (shown by red arrows) can be seen around both the pure Ti and the Zn-0.8Mn alloy scaffolds compared to 8 weeks postoperatively. Among the two, the Zn-0.8Mn alloy group showed greater new bone mass around the scaffold. Large amounts of new bone tissues and degradation products (shown by yellow arrows) can be observed around the Zn-0.8Mn alloy scaffold. In summary, the new bone tissues at the bone defect sites gradually increased with time in both groups, and numerous new bone tissues were observed around the Zn-0.8Mn alloy scaffold. Besides, the Zn-0.8Mn alloy scaffold degraded gradually with time, and the surrounding degradation products increased as the scaffold size decreased. The above results proved that the Zn-0.8Mn alloy has favorable osteogenic properties in vivo.

3.5.2. Cross-sectional and histological results

Fig. 9 illustrates the EDS mapping of pure Ti and Zn-0.8Mn alloy (12 weeks after surgery), maps of elements zinc, titanium, oxygen, calcium, phosphate, and carbon are in green, dark green, light blue, orange, yellow and gray, respectively. New bone tissue indicates by calcium and phosphate was observed beside pure Ti and Zn-0.8Mn alloy scaffolds. Besides, overlapping oxygen and zinc were observed on the surface of Zn-0.8Mn alloy scaffolds, indicates the *in vivo* corrosion products of Zn-0.8Mn alloy, zinc oxide or zinc hydroxide.

The Van Gieson staining results of rat femoral condyle defect repair in the pure Ti control group and the Zn-0.8Mn alloy group at different points are shown in Fig. 10a. Four weeks after surgery, sparse new bone tissues can be seen around both the pure Ti and Zn-0.8Mn alloy implants under low magnification. The Zn-0.8Mn alloy group showed increased bone tissue regenerations, and a small amount of new bone growth inside the porous scaffolds can be observed under high magnification. Eight weeks postoperatively, increased new bone tissues were observed around both the pure Ti and the Zn-0.8Mn alloy scaffolds under low magnification, where

the Zn-0.8Mn alloy group showed greater new bone mass around the scaffold. Additionally, the new trabecular bone was thicker, and increased bone tissue growth could be observed in the scaffold under high magnification. After 12 weeks, the new bone mass further increased in both groups, and the Zn-0.8Mn alloy group exhibited increased new bone tissue compared to the pure Ti group. Under low magnification, a large amount of new bone tissue could be observed to surround the degradation products of the Zn-0.8Mn alloy scaffold, and considerable bone ingrowth into the scaffold can be observed under high magnification. In summary, the new bone mass at the bone defect sites gradually increased with time in both groups, where the Zn-0.8Mn alloy group had greater new bone mass, and showed promising bone ingrowth characteristics, suggesting that the Zn-0.8Mn alloy promotes bone regeneration and ingrowth at bone defect sites, Fig. 10b shows the semi-quantitative analysis results of newly formed bone (BV/TV). Both groups exhibit gradually increasing new bone mass with time, and the Zn-0.8Mn alloy group showed higher increases. At 8 weeks and 12 weeks postoperatively, the Zn-0.8Mn alloy scaffold showed significantly improved bone repair properties compared to the pure Ti scaffold.

The Toluidine blue and Paragon staining results of the hard tissue slices are shown in Fig. 11. In Fig. 11a, new bone tissues were stained dark blue. The new bone mass at bone defect sites of experimental animals gradually increased with time in both groups. New bone tissues increased around the Zn-0.8Mn alloy scaffold compared to the pure Ti group at the same time-point. Both the pure Ti and Zn-0.8Mn alloy scaffolds exhibited good bone ingrowth characteristics under high magnification. The results of Toluidine blue staining were consistent with that of Van Gieson staining, which further confirmed good bone repair properties of the Zn-0.8Mn alloy scaffold. The results of Paragon staining are shown in Fig. 11b, which mainly shows tissue and cell morphologies around the pure Ti and Zn-0.8Mn alloy scaffolds. The surrounding areas of both the pure Ti and Zn-0.8Mn alloy scaffolds were filled with newly generated bone tissue, healthy adipose tissue, and a small

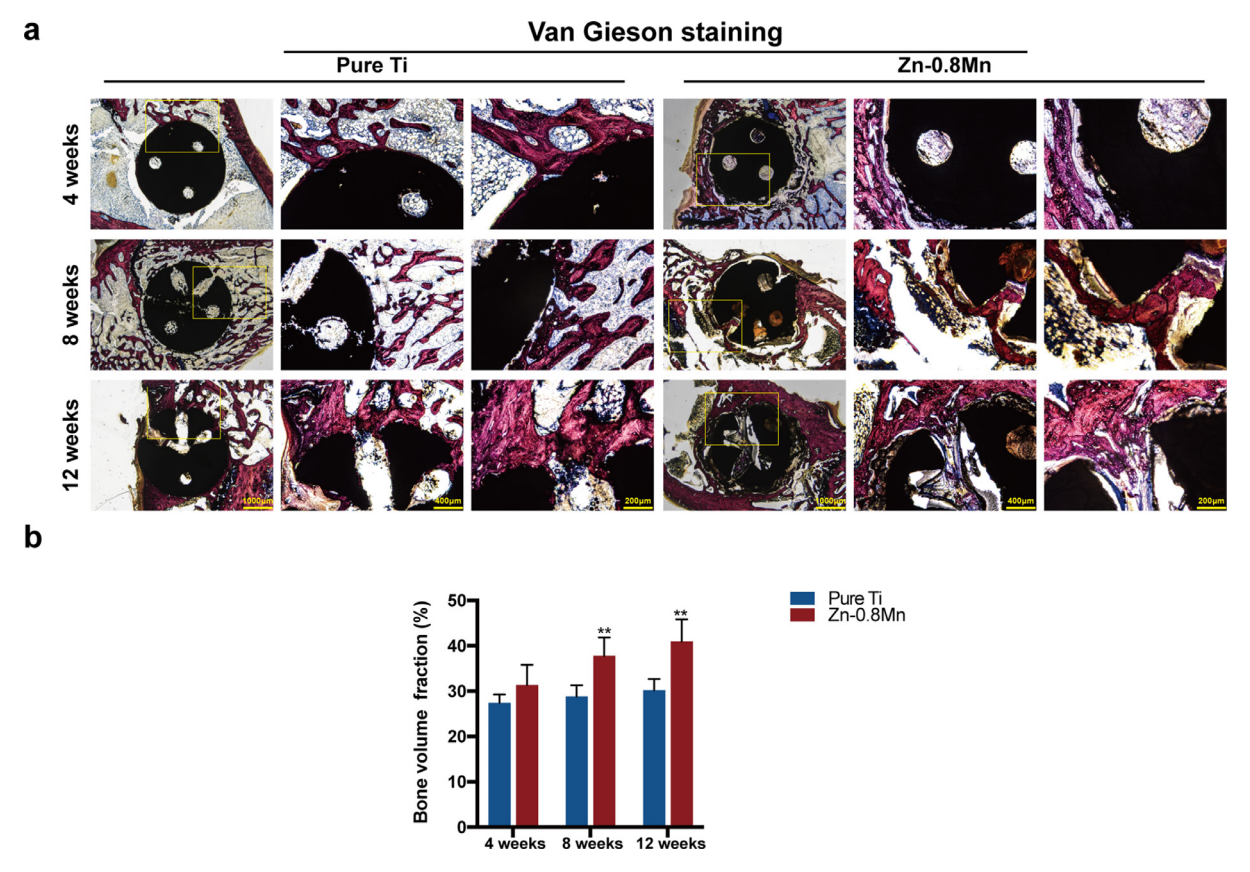


Fig. 10. (a) The Van Gieson staining results of specimens 4 weeks, 8 weeks, and 12 weeks postoperatively. Within each row, full-view images of bone defect areas $(20\times)$, medium magnification images $(50\times)$, and higher magnification images $(100\times)$ arranged from left to right. (b) The bone volume fraction (BV/TV) of pure Ti group and Zn-0.8Mn alloy group at indicated times. Data represent mean \pm standard deviation. (** p < 0.01).

amount of fibrous tissue at different time-points. Under high magnification, we observed that new bone tissue had grown into the pure Ti and Zn-0.8Mn alloy scaffolds, and no apparent inflammatory cell aggregation was observed in either group, suggesting that the Zn-0.8Mn alloy scaffold retains satisfactory local compatibility.

3.5.3. In vivo biosafety evaluation of Zn-0.8Mn alloy

Rats were euthanized 12 weeks post-surgery, and their right femurs were removed. Heart, liver, spleen, lung, and kidney tissues were sampled at the same time. The organ tissues were sliced and stained with H&E. The Zn-0.8Mn alloy group was compared to the pure Ti group to evaluate the *in vivo* biosafety. The results are shown in Fig. 12a. No noticeable abnormalities were observed in the organ tissue slices from the Zn-0.8Mn alloy group, compared to the pure Ti control group. Fig. 12b shows the comparison between the ion concentrations of Zn²⁺ and Mn²⁺ in rat blood and organs collected from the Zn-0.8Mn alloy group and pure Ti group. The results showed no abnormal increases in Zn²⁺ and Mn²⁺ ion concentrations in either the blood or organs, thereby illustrating that the Zn-0.8Mn alloy retains desirable *in vivo* biosafety and presents no ion accumulation in organs.

4. Discussion

In this study, the Mn element, which has promising biocompatibility and osteogenic activity, was chosen as the alloying element. The addition of a trace amount of Mn not only improved the mechanical strength of pure Zn but also significantly increased its elongation rate. The addition of Mn significantly improved the cytocompatibility of Zn. As showed in Figs. 4 and 5, the improved cytocompatibility of Zn-Mn alloys compared to Zn was confirmed

by cell proliferation activity, Live/Dead, and cytoskeletal staining results. More important, the Zn-Mn alloys exhibit satisfactory osteogenic properties both in vitro and in vivo. As shown in Figs. 6 and 7, in vitro osteogenic properties of degradable Zn-Mn alloys were evaluated based on three aspects, namely the quantitative analysis of ALP activity, ALP activity staining, and expression levels of osteogenic-related genes. ALP activities of the Zn-Mn alloy extract-induced groups improved compared to the blank control and pure Zn groups at all time-points, with Zn-0.8Mn alloy exhibiting the best results (Fig. 6). Furthermore, expression levels of osteogenic marker genes (ALP, Col I, OCN, and Runx-2) in the extract-induced differentiated MC3T3-E1 cells indicate improved gene expression in the Zn-Mn alloy groups in comparison to the blank control group (Fig. 7). This further confirmed the osteogenic activity of Zn-Mn alloys and provided theoretical support at the genetic level. In summary, it was verified in vitro that Zn-Mn alloys exerted functional osteogenic activities, which provide significant benefits for their application as orthopedic implant materials.

We believe that the better osteogenic activity of Zn-Mn alloys compared with pure Zn mainly due to the following factors. On the one hand, the addition of trace Mn endows Zn-Mn alloys with satisfactory cytocompatibility. Mn element is an essential trace element in the human body. It mainly acts as a coenzyme in a variety of basic life processes, including, but not limited to, energy metabolism, new bone formation, free radical scavenging, and synthesis of neurotransmitters [52,53]. Mn can regulate the interaction between cells and the extracellular matrix by affecting integrin activity, which in turn affects cell proliferation, adhesion, and spreading [53]. Studies have shown that there are threshold effects of Zn²⁺ and Mn²⁺ ion on cell proliferation activity. High concentration of Zn²⁺ (higher than 3.9–5.2 μ g/mL) [54,55] and

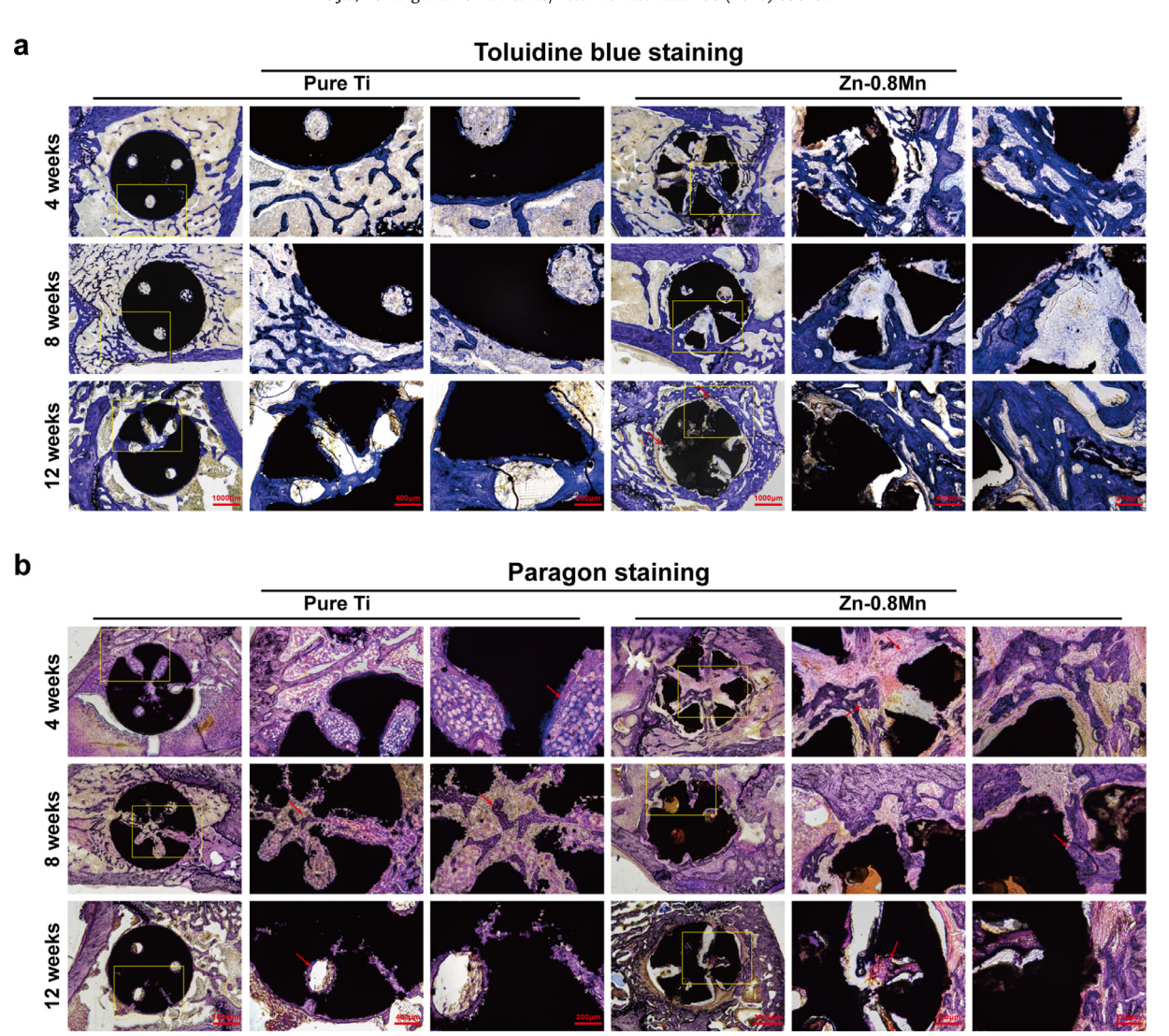


Fig. 11. The Toluidine blue staining and paragon staining results of hard tissue sections. Within each group, full-view images of bone defect areas $(20\times)$, medium magnification images $(50\times)$ and high magnification images $(100\times)$ arranged from left to right. (a) The Toluidine blue staining results of pure Ti group and Zn-0.8Mn alloy group, red arrows indicate the biodegradable products of Zn-0.8Mn alloy scaffolds at 12 weeks postoperatively. (b) The paragon staining results of pure Ti group and Zn-0.8Mn alloy group, promising bone ingrowth (red arrows), normal morphology of bone tissue, regenerative bone, cartilage, and fat tissue were observed. (For interpretation of the references to colour in this figure legend, the reader is referred to the web version of this article.)

 Mn^{2+} (>0.1 mM MnCl₂) [56] are detrimental to cell proliferation. According to the ion concentration test results of the pure Zn and Zn-Mn alloy extracts (Table 1), there was no significant difference in the Zn²⁺ concentrations between the two groups, all about 13 μ g/mL (n = 5). This explains the inferior cell proliferation and ALP activity results of pure Zn after diluting the extracts to 1-folds (Zn²⁺about 6.5 μg/mL) while the cell proliferation and ALP activity of pure Zn groups improved after diluting the extracts to 2-folds (about 3.25 μ g/mL) in Figs. 4 and 6. However, favorable cell proliferation, spreading and osteogenic properties were achieved in 1-fold diluted extracts in Zn-Mn alloy groups. Considering the positive effects of trace amounts of Mn²⁺ on cell proliferation, adhesion and spreading, it is reasonable to believe that the released Mn²⁺ ion exerted a positive effect on the cytocompatibility and significantly optimized its biocompatibility of pure Zn. On the other hand, Mn also plays positive roles during bone metabolism. Studies have confirmed that Mn can upregulate expression of osteogenesis-related genes such as ALP and BMP, promote collagen fiber regeneration and deposition, regulate bone remodeling and maintain the bone mass [44-47]. Therefore, the Mn²⁺ in Zn-Mn alloy extracts may directly upregulate osteogenic gene expression

and ALP activity, inducing better osteogenic properties in contrast to pure Zn. In addition, both Zn and Mn are essential trace elements that play an active role in bone metabolism. Whether there is a synergistic effect between Zn and Mn ions in regulating bone metabolism attracts our attention. However, to date, no relevant literature was found. Further research is warranted to clarify whether Zn and Mn ions exert synergistic bone-promoting effects.

To verify the *in vitro* results of Zn-Mn alloys, the Zn-0.8Mn alloy with the best comprehensive property was selected for *in vivo* study. A bone defect model at partial load-bearing regions (rat femur condyle) was established considering the osteogenic property of Zn-Mn alloy. In order to evaluate the bone defect repair activity, pure Ti, the golden clinical standard material for extensive bone defect repair, was selected as the control in this study. According to Micro-CT results (Fig. 8), the Zn-0.8Mn alloy group showed increased new bone tissue and thicker trabecular bones at the same time-points. Van Gieson staining of hard tissue slices agreed with micro-CT scans, in that the Zn-0.8Mn alloy scaffolds showed better bone repair capability and good bone ingrowth characteristics. Toluidine blue staining results indicated that the Zn-0.8Mn alloy scaffold was surrounded by increased new bone tissue. A

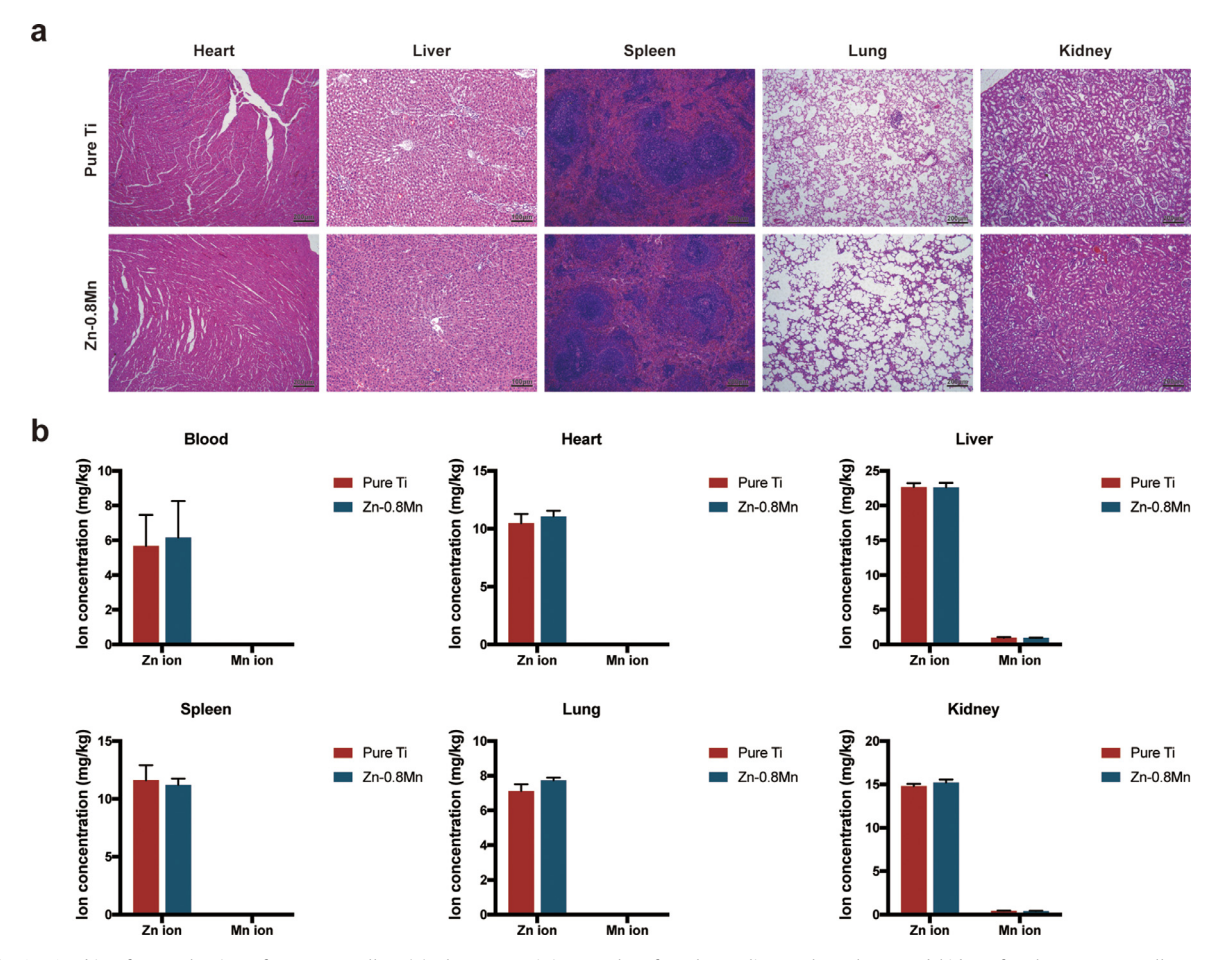


Fig. 12. The *in vivo* biosafety evaluation of Zn-0.8Mn alloy. (a) The H&E staining results of rat heart, liver, spleen, lung, and kidney for the Zn-0.8Mn alloy group and the pure Ti group. (b) The ion concentration of Zn^{2+} and Mn^{2+} in rat blood and organs from the Zn-0.8Mn alloy group and the pure Ti group.

large amount of new bone grew into the Zn-0.8Mn alloy scaffold, showing good bone regeneration promotion and bone ingrowth. Furthermore, Paragon staining results confirmed mild degradation behavior of the Zn-0.8Mn alloy and its superior local compatibility. Consistent with the *in vitro* results, the Zn-0.8Mn alloy showed beneficial osteogenic properties *in vivo*. As an element with biphasic osteogenic activity, the implantation of Zn-containing materials at the bone defect sites both promoted bone regeneration and inhibited bone resorption by osteoclasts, thereby resulting in greater new bone mass and thicker new trabecular bones.

In summary, the biodegradable Zn-Mn alloys satisfy the basic requirements of ideal orthopedic implant materials. It exhibits not only suitable material properties but also superior biocompatibility and biological functions. Therefore, it can be expected to be applied in various clinical scenarios. Firstly, considering the favorable osteogenic activity and plasticity of Zn-Mn alloys, they can be designed as porous implants of different shapes for bone defects repair, besides, the Zn-Mn alloys possess superior mechanical properties compared to the traditional bone substitution materials, such as HA, CaP, biodegradable polymers (PCL, PLA, PLGA, etc.), which make it particularly suitable for segmental bone defects repair. Secondly, biodegradable Zn-Mn alloys can be manufactured into implants designed for a variety of clinical applications, including screws for fracture fixation, intramedullary nails for long bone shaft fracture fixation or biodegradable interference screws for ligaments injury repair. At the early stage of implantation, the Zn-Mn alloys implants can serve as a mechanical support and slow corelease of Zn²⁺ and Mn²⁺, which promotes osteogenic activity and bone injury repair. As it completes its mechanical and biological functions, it will degrade gradually until it is completely metabolized or absorbed.

5. Conclusions

Here, a trace amount of Mn element, with different mass fractions, was added into pure Zn to prepare biodegradable Zn-Mn alloys. The addition of Mn enhanced the mechanical properties of pure Zn, especially the elongation, which reached $83.96\pm2.36\%$ for Zn-0.8Mn alloy. The addition of Mn significantly improved the cytocompatibility and osteogenic properties of pure Zn. *In vitro*, the Zn-Mn alloy could promote MC3T3-E1 cell proliferation, adhesion, spreading and osteogenic differentiation. Furthermore, the rat femoral condyle defect repair experiment confirmed the superior osteogenic properties of the Zn-0.8Mn alloy *in vivo*. Therefore, Zn-Mn alloy can be expected to become a new option for orthopedic implant materials, especially in the field of bone defect or fracture repair.

Declaration of Competing Interests

The authors declare no competing financial interests or personal relationships.

Acknowledgments

This work was financially supported by the Natural Science Foundation of China [grant numbers 51931001]. Bo Jia, Hongtao Yang, and Yu Han contributed equally to this study.

Supplementary materials

Supplementary material associated with this article can be found, in the online version, at doi:10.1016/j.actbio.2020.03.009.

References

- [1] P. Xiong, Z. Jia, W. Zhou, J. Yan, P. Wang, W. Yuan, Y. Li, Y. Cheng, Z. Guan, Y. Zheng, Osteogenic and pH stimuli-responsive self-healing coating on biomedical Mg-1Ca alloy, Acta Biomater. 92 (2019) 336–350.
- [2] P. Xiong, J. Yan, P. Wang, Z. Jia, W. Zhou, W. Yuan, Y. Li, Y. Liu, Y. Cheng, D. Chen, Y. Zheng, A pH-sensitive self-healing coating for biodegradable magnesium implants, Acta Biomater 98 (2019) 160–173.
- [3] A. Kafri, S. Ovadia, G. Yosafovich-Doitch, E. Aghion, The effects of 4% Fe on the performance of pure Zinc as biodegradable implant material, Ann. Biomed. Eng. 47 (2019) 1400–1408.
- [4] X. Tong, D. Zhang, X. Zhang, Y. Su, Z. Shi, K. Wang, J. Lin, Y. Li, J. Lin, C. Wen, Microstructure, mechanical properties, biocompatibility, and in vitro corrosion and degradation behavior of a new Zn-5Ge alloy for biodegradable implant materials, Acta Biomater. 82 (2018) 197–204.
- [5] C. Liu, Z. Ren, Y. Xu, S. Pang, X. Zhao, Y. Zhao, Biodegradable magnesium alloys developed as bone repair materials: a review, Scanning 2018 (2018) 9216314.
- [6] M. Li, P. Wan, W. Wang, K. Yang, Y. Zhang, Y. Han, Regulation of osteogenesis and osteoclastogenesis by zoledronic acid loaded on biodegradable magnesium-strontium alloy, Sci. Rep. 9 (2019) 933.
- [7] X. Kong, L. Wang, G. Li, X. Qu, J. Niu, T. Tang, K. Dai, G. Yuan, Y. Hao, Mg-based bone implants show promising osteoinductivity and controllable degradation: a long-term study in a goat femoral condyle fracture model, Mater. Sci. Eng., C 86 (2018) 42–47.
- [8] W. Jiang, A.F. Cipriano, Q. Tian, C. Zhang, M. Lopez, A. Sallee, A. Lin, M.C. Cortez Alcaraz, Y. Wu, Y. Zheng, H. Liu, *In vitro* evaluation of MgSr and MgCaSr alloys via direct culture with bone marrow-derived mesenchymal stem cells, Acta Biomater. 72 (2018) 407–423.
- [9] H. Nygren, N. Bigdeli, L. Ilver, P. Malmberg, Mg-corrosion, hydroxyapatite, and bone healing, Biointerphases 12 (2017) 02C407.
- [10] E. Mostaed, M. Sikora-Jasinska, J.W. Drelich, M. Vedani, Zinc-based alloys for degradable vascular stent applications, Acta Biomater 71 (2018) 1–23.
- [11] P.K. Bowen, E.R. Shearier, S. Zhao, R.J. Guillory 2nd, F. Zhao, J. Goldman, J.W. Drelich, Biodegradable metals for cardiovascular stents: from clinical concerns to recent Zn-alloys, Adv. Healthcare Mater. 5 (2016) 1121–1140.
- [12] L. Tian, Y. Sheng, L. Huang, D.H. Chow, W.H. Chau, N. Tang, T. Ngai, C. Wu, J. Lu, L. Qin, An innovative Mg/Ti hybrid fixation system developed for fracture fixation and healing enhancement at load-bearing skeletal site, Biomaterials 180 (2018) 173–183.
- [13] Y. Liu, Y. Wu, D. Bian, S. Gao, S. Leeflang, H. Guo, Y. Zheng, J. Zhou, Study on the Mg-Li-Zn ternary alloy system with improved mechanical properties, good degradation performance and different responses to cells, Acta Biomater. 62 (2017) 418–433.
- [14] D. Tie, R. Guan, H. Liu, A. Cipriano, Y. Liu, Q. Wang, Y. Huang, N. Hort, An in vivo study on the metabolism and osteogenic activity of bioabsorbable Mg-1Sr alloy, Acta Biomater. 29 (2016) 455-467.
- [15] Y. Li, L. Liu, P. Wan, Z. Zhai, Z. Mao, Z. Ouyang, D. Yu, Q. Sun, L. Tan, L. Ren, Z. Zhu, Y. Hao, X. Qu, K. Yang, K. Dai, Biodegradable Mg-Cu alloy implants with antibacterial activity for the treatment of osteomyelitis: in vitro and in vivo evaluations, Biomater. 106 (2016) 250–263.
- [16] M. Ezechieli, H. Meyer, A. Lucas, P. Helmecke, C. Becher, T. Calliess, H. Windhagen, M. Ettinger, Biomechanical properties of a novel biodegradable magnesium-based interference screw, Orthop. Res. Rev. 8 (2016) 6445.
- [17] H. Klauser, Internal fixation of three-dimensional distal metatarsal I osteotomies in the treatment of hallux valgus deformities using biodegradable magnesium screws in comparison to titanium screws, Foot. Ankle. Surg. 25 (2019) 398–405.
- [18] Y.F. Zheng, X.N. Gu, F. Witte, Biodegradable metals, Mater. Sci. Eng., R 77 (2014) 1–34.
- [19] X.N. Gu, N. Li, Y.F. Zheng, F. Kang, J.T. Wang, L. Ruan, *In vitro* study on equal channel angular pressing AZ31 magnesium alloy with and without back pressure, Mater. Sci. Eng., B 176 (2011) 1802–1806.
- [20] V.K. Thakur, M.K. Thakur, R.R. Kessler, Biodegradable and bioabsorbable materials for osteosynthesis applications: state-of-the-art and future perspectives, Handbook of Composites from Renewable Materials, 2017, pp. 109–143.
- [21] D. Bian, W. Zhou, Y. Liu, N. Li, Y. Zheng, Z. Sun, Fatigue behaviors of HP-Mg, Mg-Ca and Mg-Zn-Ca biodegradable metals in air and simulated body fluid, Acta Biomater. 41 (2016) 351–360.
- [22] Y. Yang, P. Wu, Q. Wang, H. Wu, Y. Liu, Y. Deng, Y. Zhou, C. Shuai, The enhancement of mg corrosion resistance by alloying Mn and laser-melting, Materials (Basel) 9 (2016).
- [23] H.R. Bakhsheshi-Rad, E. Hamzah, A.F. Ismail, Z. Sharer, M.R. Abdul-Kadir, M. Daroonparvar, S.N. Saud, M. Medraj, Synthesis and corrosion behavior of a hybrid bioceramic-biopolymer coating on biodegradable Mg alloy for orthopedic implants, J. Alloys Compd. 648 (2015) 1067–1071.
- [24] W.R. Zhou, Y.F. Zheng, M.A. Leeflang, J. Zhou, Mechanical property, biocorrosion and *in vitro* biocompatibility evaluations of Mg-Li-(Al)-(Re) alloys for future cardiovascular stent application, Acta Biomater. 9 (2013) 8488–8498.

- [25] X.N. Gu, N. Li, W.R. Zhou, Y.F. Zheng, X. Zhao, Q.Z. Cai, L. Ruan, Corrosion resistance and surface biocompatibility of a microarc oxidation coating on a Mg-Ca alloy. Acta Biomater. 7 (2011) 1880–1889.
- [26] Y. Su, K. Wang, J. Gao, Y. Yang, Y.-X. Qin, Y. Zheng, D. Zhu, Enhanced cytocompatibility and antibacterial property of zinc phosphate coating on biodegradable zinc materials, Acta Biomater. 98 (2019) 174–185.
 [27] X. Shen, Y. Zhang, P. Ma, L. Sutrisno, Z. Luo, Y. Hu, Y. Yu, B. Tao, C. Li, K. Cai,
- [27] X. Shen, Y. Zhang, P. Ma, L. Sutrisno, Z. Luo, Y. Hu, Y. Yu, B. Tao, C. Li, K. Cai, Fabrication of magnesium/zinc-metal organic framework on titanium implants to inhibit bacterial infection and promote bone regeneration, Biomater. 212 (2019) 1–16.
- [28] S. Lin, X. Ran, X. Yan, W. Yan, Q. Wang, T. Yin, J.G. Zhou, T. Hu, G. Wang, Corrosion behavior and biocompatibility evaluation of a novel zinc-based alloy stent in rabbit carotid artery model, J. Biomed. Mater. Res., Part B 107 (2018) 1814–1823.
- [29] P. Li, C. Schille, E. Schweizer, E. Kimmerle-Muller, F. Rupp, A. Heiss, C. Legner, U.E. Klotz, J. Geis-Gerstorfer, L. Scheideler, Selection of extraction medium influences cytotoxicity of zinc and its alloys, Acta Biomater 98 (2019) 235–245.
- [30] L. Fong, K. Tan, C. Tran, J. Cool, M.A. Scherer, R. Elovaris, P. Coyle, B.K. Foster, A.M. Rofe, C.J. Xian, Interaction of dietary zinc and intracellular binding protein metallothionein in postnatal bone growth, Bone 44 (2009) 1151–1162.
- [31] J.C. Leek, J.B. Vogler, M.E. Gershwin, M.S. Golub, L.S. Hurley, A.G. Hendrickx, Studies of marginal zinc deprivation in rhesus monkeys. V. Fetal and infant skeletal effects, Am. J. Clin. Nutr. 40 (1984) 1203–1212.
- [32] K.A. McCall, C. Huang, C.A. Fierke, Function and mechanism of zinc metalloenzymes, J. Nutr. 130 (2000) 1437s-1446s.
- [33] M. Yamaguchi, Role of nutritional zinc in the prevention of osteoporosis, Mol. Cell. Biochem. 338 (2010) 241–254.
- [34] A.S. Tiffany, D.L. Gray, T.J. Woods, K. Subedi, B.A.C. Harley, The inclusion of zinc into mineralized collagen scaffolds for craniofacial bone repair applications, Acta Biomater. 93 (2019) 86–96.
- [35] K.H. Park, Y. Choi, D.S. Yoon, K.M. Lee, D. Kim, J.W. Lee, Zinc promotes osteoblast differentiation in human mesenchymal stem cells via activation of the cAMP-PKA-CREB signaling pathway, Stem Cells Dev. 27 (2018) 1125–1135.
- [36] X. Fu, Y. Li, T. Huang, Z. Yu, K. Ma, M. Yang, Q. Liu, H. Pan, H. Wang, J. Wang, M. Guan, Runx2/Osterix and Zinc uptake synergize to orchestrate osteogenic differentiation and citrate containing bone apatite formation, Adv. Sci. (Weinheim, Germany) 5 (2018) 1700755.
- [37] W. Yu, T.W. Sun, C. Qi, Z. Ding, H. Zhao, S. Zhao, Z. Shi, Y.J. Zhu, D. Chen, Y. He, Evaluation of zinc-doped mesoporous hydroxyapatite microspheres for the construction of a novel biomimetic scaffold optimized for bone augmentation, Int. J. Nanomed. 12 (2017) 2293–2306.
- [38] H. Yang, X. Qu, W. Lin, D. Chen, D. Zhu, K. Dai, Y. Zheng, Enhanced osseointe-gration of Zn-Mg composites by tuning the release of Zn ions with sacrificial mg-rich anode design, ACS Biomater. Sci. Eng. 5 (2018) 453–467.
- [39] C. Xiao, L. Wang, Y. Ren, S. Sun, E. Zhang, C. Yan, Q. Liu, X. Sun, F. Shou, J. Duan, H. Wang, G. Qin, Indirectly extruded biodegradable Zn-0.05 wt%Mg alloy with improved strength and ductility: in vitro and in vivo studies, J. Mater. Sci. Technol. (Shenyang, China) 34 (2018) 1618–1627.
- [40] H.F. Li, X.H. Xie, Y.F. Zheng, Y. Cong, F.Y. Zhou, K.J. Qiu, X. Wang, S.H. Chen, L. Huang, L. Tian, L. Qin, Development of biodegradable Zn-Lx binary alloys with nutrient alloying elements Mg, Ca and Sr, Sci. Rep. 5 (2015) 10719.
- [41] S. Sun, Y. Ren, L. Wang, B. Yang, H. Li, G. Qin, Abnormal effect of Mn addition on the mechanical properties of as-extruded Zn alloys, Mater. Sci. Eng. A 701 (2017) 129–133.
- [42] W. Fujitani, Y. Hamada, N. Kawaguchi, S. Mori, K. Daito, A. Uchinaka, T. Matsumoto, Y. Kojima, M. Daito, T. Nakano, N. Matsuura, Synthesis of hydrox-yapatite containing manganese and its evaluation of biocompatibility, Nano Biomed. 2 (2010) 37–46.
- [43] P.M. Torres, S.I. Vieira, A.R. Cerqueira, S. Pina, O.A. da Cruz Silva, J.C. Abrantes, J.M. Ferreira, Effects of Mn-doping on the structure and biological properties of beta-tricalcium phosphate, J. Inorg. Biochem. 136 (2014) 57–66.
- [44] M. Miola, C.V. Brovarone, G. Maina, F. Rossi, L. Bergandi, D. Ghigo, S. Saracino, M. Maggiora, R.A. Canuto, G. Muzio, E. Vernè, *In vitro* study of manganesedoped bioactive glasses for bone regeneration, Mater. Sci. Engi. C 38 (2014) 107-118
- [45] L. Yu, Y. Tian, Y. Qiao, X. Liu, Mn-containing titanium surface with favorable osteogenic and antimicrobial functions synthesized by PIII&D, Colloids. Surf., B 152 (2017) 376–384.
- [46] B.J. Friedman, J.H. Freeland-Graves, C.W. Bales, F. Behmardi, R.L. Shorey-Kutschke, R.A. Willis, J.B. Crosby, P.C. Trickett, S.D. Houston, Manganese balance and clinical observations in young men fed a manganese-deficient diet, J. Nutr. 117 (1) (1987) 133–143.
- [47] Y.J. Bae, M.H. Kim, Manganese supplementation improves mineral density of the spine and femur and serum osteocalcin in rats, Biol. Trace Elem. Res. 124 (2008) 28–34.
- [48] N.Z. Baquer, M. Sinclair, S. Kunjara, U.C. Yadav, P. McLean, Regulation of glucose utilization and lipogenesis in adipose tissue of diabetic and fat fed animals: effects of insulin and manganese, J. Biosci. 28 (2003) 215–221.
- [49] J. Hreha, A. Wey, C. Cunningham, E.S. Krell, E.A. Brietbart, D.N. Paglia, N.J. Montemurro, D.A. Nguyen, Y.J. Lee, D. Komlos, E. Lim, J. Benevenia, J.P. O'Connor, S.S. Lin, Local manganese chloride treatment accelerates fracture healing in a rat model. I. Orthon. Res. 33 (2015) 122–130.
- [50] H. Yang, X. Qu, W. Lin, C. Wang, D. Zhu, K. Dai, Y. Zheng, In vitro and in vivo studies on zinc-hydroxyapatite composites as novel biodegradable metal matrix composite for orthopedic applications, Acta Biomater. 71 (2018) 200– 214.

- [51] H. Yang, B. Jia, Z. Zhang, X. Qu, G. Li, W. Lin, D. Zhu, K. Dai, Y. Zheng, Alloying design of biodegradable zinc as promising bone implants for load-bearing applications, Nat. Commun. 11 (1) (2020) 401.

 [52] K.M. Erikson, M. Aschner, Manganese: its role in disease and health, Met. lons
- Life Sci. (2019) 19.
- [53] B.R. Barrioni, E. Norris, S. Li, P. Naruphontjirakul, J.R. Jones, M.M. Pereira, Osteogenic potential of sol-gel bioactive glasses containing manganese, J. Mater. Sci. Mater. Med. 30 (2019) 86.

- [54] J. Ma, N. Zhao, D. Zhu, Endothelial cellular responses to biodegradable metal Zinc, ACS Biomater. Sci. Eng. 1 (2015) 1174–1182.
 [55] J. Ma, N. Zhao, D. Zhu, Bioabsorbable zinc ion induced biphasic cellular responses in vascular smooth muscle cells, Sci. Rep. 6 (2016) 26661.
 [56] B.R. Barrioni, A.C. Oliveira, M.D. Leite, M.D. Pereira, Sol-gel-derived manganese-releasing bioactive glass as a therapeutic approach for bone tissue engineering, J. Mater. Sci. 52 (2017) 8904–8927.